Elliptic Flow Differences between Baryons and Anti-Baryons in Heavy-Ion Collisions Using SMASH Model

Shuai Zhou and Shusu Shi*

Key Laboratory of Quark and Lepton Physics (MOE) and Institute of Particle Physics, Central China Normal University, Wuhan 430079, China

(Received 6 December 2024; accepted manuscript online 20 January 2025)

Significant differences exist in the elliptic flow v_2 for particles and their corresponding anti-particles. These differences, which are more significant for baryons and anti-baryons, were observed from the solenoidal tracker (STAR) experiment during Beam Energy Scan I (BES-I) at relativistic heavy ion collider (RHIC). By employing the simulated many-accelerated strongly interacting hadrons (SMASH) model, we studied the v_2 differences between protons and anti-protons as well as between Λ and $\bar{\Lambda}$ in Au + Au collisions at $\sqrt{s_{\rm NN}} = 7.7\,{\rm GeV}$ as a function of the evolution time. It was found that as the evolution time increases, the v_2 differences between protons and anti-protons become more significant than those between Λ and $\bar{\Lambda}$. This phenomenon can be explained by the different constituent quarks of protons and Λ. Given that some of the u and d quarks come from the colliding nuclei and are transported to midrapidity, they undergo more interactions than the produced quarks, resulting in protons Δv_2 being larger than Λ Δv_2. We compared the SMASH calculations with STAR BES-I data and concluded that higher-precision data from BES-II will set constraints on theoretical frameworks to interpret the v_2 differences between particles and anti-particles.

DOI: 10.1088/0256-307X/42/2/021201 CSTR: 32039.14.0256-307X.42.2.021201

1. Introduction. During high-energy heavy-ion collisions, extreme temperature and density conditions are reached, which facilitates the study of strongly interacting matter. One of the most significant phenomena observed in such collisions is a collective flow (v_n), which refers to the correlated motion of particles produced during the collisions. This collective flow provides essential information about the early-stage dynamics of the system, equation of state (EoS), and transport properties of the medium. In heavy-ion collisions, the produced particles do not scatter isotropically, as expected in a purely thermal system. Instead, they exhibit a pattern of anisotropic distribution in momentum space driven by the pressure gradients generated in the initial stages of the collisions. This anisotropy, which is commonly decomposed into harmonic coefficients, offers insights into the response of the medium to the initial geometric asymmetries.[1,2] Thus, the collective flow plays an important role in understanding the evolution of the system by connecting microscopic interactions to macroscopic observable effects. Not only does it provide a window into the properties of strongly interacting matter but also serves as a key observable in constraining theoretical models of collision dynamics.[3–20]

An elliptic flow, denoted by v_2, measures the anisotropic distribution of particles produced in the azimuthal direction with respect to the reaction plane ($\Psi_{\rm rp}$) in heavy-ion collisions. This is defined as the second Fourier coefficient in the Fourier decomposition of the particle yield as a function of the azimuthal angle:[1]

$$E\frac{d^3N}{d^3p} = \frac{1}{2\pi}\frac{d^2N}{p_{\rm T}dp_{\rm T}dy}\Big(1 + \sum_{n=1}^{\infty} 2v_n \cos[n(\phi - \Psi_{\rm rp})]\Big), \quad (1)$$

where ϕ denotes the azimuthal angle of the final-state particles in the laboratory frame. The quantity v_2 is driven by the initial geometric anisotropy. Specifically, in non-central collisions, where the overlap region is elliptical rather than circular, the anisotropies in the particle momentum distributions originate from the initial asymmetries in the geometry of the system, leading to the formation of v_2. Thus, v_2 is a valuable probe for studying the degrees of freedom of nuclear matter created in heavy-ion collisions.[21–24] Such degrees of freedom, whether dominated by partonic or hadronic interactions, are crucial for understanding QCD phase transitions.[25,26] In addition, the energy dependence of the in-medium correction factor for the in-medium nucleon–nucleon elastic cross section has a significant impact on collective flows.[27] Comparing experimental v_2 data with theoretical calculations provides information about the degrees of freedom achieved in heavy-ion collisions and further constrains the EoS of nuclear matter.[27–34]

The STAR collaboration has measured v_2 for identified particles at midrapidity in Au + Au collisions as part of the Beam Energy Scan program at the relativistic heavy ion collider (RHIC), with collision energies ranging from 7.7 to 62.4 GeV.[35–38] Collision energy-dependent differences in v_2 between particles and their corresponding anti-particles were observed. These differences increase with decreasing beam energy and are more significant for baryons than

*Corresponding author. Email: shiss@ccnu.edu.cn

© 2025 Chinese Physical Society and IOP Publishing Ltd. All rights, including for text and data mining, AI training, and similar technologies, are reserved.

for mesons. These results suggest that, at lower energies, particles and anti-particles do not exhibit the universal number-of-constituent-quark scaling of v_2 observed at 200 GeV.[9,10,12,39]

Some models explain the v_2 differences from distinct perspectives. Within the framework of the UrQMD model, tracing the number of initial quarks in protons partly accounts for the difference in v_2 between transported protons and anti-protons, providing an explanation for the observed differences in the Beam Energy Scan program at RHIC.[40] In a hybrid model, the fluid dynamical evolution of the fireball is combined with a transport treatment for both the initial and final hadronic phases. It has been found that the propagation of the baryon-number current during hydrodynamic evolution as well as the transport treatment of the hadronic phase are essential for reproducing experimental data.[41] In the context of the quark coalescence model, because of baryon stopping, especially at lower energies, different constituent quarks exhibit varying v_2. In addition, different transport properties lead to distinct interactions between quarks, resulting in different v_2 values.[42] Thus, v_2 differences remain an area of active research.[43–47] However, owing to the limitations imposed by the statistical constraints of the data, we cannot draw clear conclusions regarding such differences among different baryon types, particularly the relationship between the v_2 differences of protons and Λ, according to the STAR Beam Scan I results.[35–38]

In this study, we focused on the relationship describing the v_2 differences between protons and Λ using the simulated many-accelerated strongly interacting hadrons (SMASH) model. Because the v_2 differences are significant at 7.7 GeV, which is the lowest collision energy among RHIC-STAR Au+Au collisions, we chose this energy for our study. We investigated the v_2 differences between protons and Λ for different centralities and at different times during the collision evolution, specifically at 2 fm/c, 10 fm/c, and 50 fm/c after the collision. By comparing the v_2 differences between protons and Λ at these specific times during the collision evolution, we aimed to elucidate the dependence of the v_2 differences on both transported and produced quarks, as well as on the quark flavor in baryons. In addition, we propose a method to re-examine the mechanisms that explain the v_2 differences for different models.

The remainder of this paper is organized as follows. The SMASH model is introduced in Section 2. In Section 3, we discuss the relationship between v_2 and the collision evolution time, along with its physical interpretation. Finally, a summary is presented in Section 4.

2. SMASH Model. Various theoretical frameworks have been developed to model the dynamics of heavy-ion collisions. The SMASH model is a state-of-the-art hadronic transport approach that simulates the late-stage hadronic interactions following the partonic stage.[48,49] Research advances within the SMASH framework have boosted the understanding of the dynamics of heavy-ion collisions. Specifically, SMASH has been instrumental in elucidating the mechanisms of light nuclei formation, baryon stopping, and generation of anisotropies in momentum space. By integrating advanced models such as CRAB for coalescence studies[50] and employing sophisticated parameterizations of shear viscosity η/s,[51] SMASH has successfully reproduced experimental observations of particle correlations and flow patterns[52]. These advances underscore the capability of the model to accurately describe the complex physics of heavy-ion collisions across a wide range of energies. In addition, they contribute to a deeper understanding of the QCD phase diagram and properties of nuclear matter under extreme conditions. Future enhancements will focus on refining the initial conditions and improving the EoS parameterization, further strengthening the role of SMASH in advancing our knowledge of strong interaction dynamics.[53]

SMASH incorporates a comprehensive treatment of hadronic interactions, including binary collisions, resonance decay, and propagation of hadrons through the medium. It is particularly suitable for low-energy heavy-ion collisions and provides a detailed description of the freeze-out process and development of the collective flow.[54] For the specific scenario of 7.7 GeV Au + Au collisions, we selected time points at 2 fm/c, 10 fm/c, and 50 fm/c as the endpoints of the cascade mode simulation. In the context of the system evolution, the early stage is characterized by a timescale of approximately 2 fm/c. The intermediate to late stages are associated with a duration of approximately 10 fm/c, whereas the final stage of the evolution of the system is defined by a timescale of approximately 50 fm/c. These time points represent key stages in the evolution of a collision, allowing for the study of the dynamics of particle interactions and development of the collective flow.[55] By employing a consistent time step size and focusing on these specific time points, we aimed to obtain a comprehensive understanding of the evolution of the system while maintaining computational efficiency. We calculated the elliptic flow using the expression $v_2 = \cos(2\phi)$, because the azimuth of the reaction plane is set to zero in the model. Event centrality is defined based on the collision impact parameter because, in the early stages of a collision, the production of particles is not yet fully formed. Therefore, it is not appropriate to define the centrality using the reference multiplicity of the final-state particles.

3. Results and Discussion. The duration of the collision evolution is referred to as the evolution time. We calculated the v_2 differences by subtracting the value of v_2 of the particles from that of their corresponding anti-particles within each transverse momentum (p_{T}) bin. Subsequently, a fitting procedure was employed to determine the mean v_2 difference by analyzing the individual v_2 differences over a p_{T} range from 0.6 to 2.3 GeV/c, similar to the method used in the STAR experiment.[35–37] This approach enables the characterization of the v_2 difference between particles and anti-particles over a range of momenta, thereby providing insights into the asymmetries in the azimuthal anisotropy of the final-state particles.

Figure 1 shows the proton v_2 and Λ v_2 differences at an evolution time of 10 fm/c in Au+Au collisions at $\sqrt{s_{\mathrm{NN}}} =$ 7.7 GeV. Upper panels (a), (b), (c), and (d) show v_2 for protons Λ and their corresponding anti-particles. Protons

and anti-protons are indicated by squares, whereas Λ and $\bar{\Lambda}$ are denoted by triangles. Lower panels (a1), (b1), (c1), and (d1) show the proton v_2 and Λ v_2 differences for each p_{T} bin. Our results reveal that, across different centrality bins, the v_2 differences for protons are generally greater than those for Λ. At an evolution time of 10 fm/c, the majority of particles undergo freeze-out, and the interactions among them diminish significantly, leading to the stabilization of v_2 differences. By examining the v_2 differences between protons and Λ particles at this stage of evolution, we aimed to investigate the influence of different quark compositions on the observed v_2 variations.

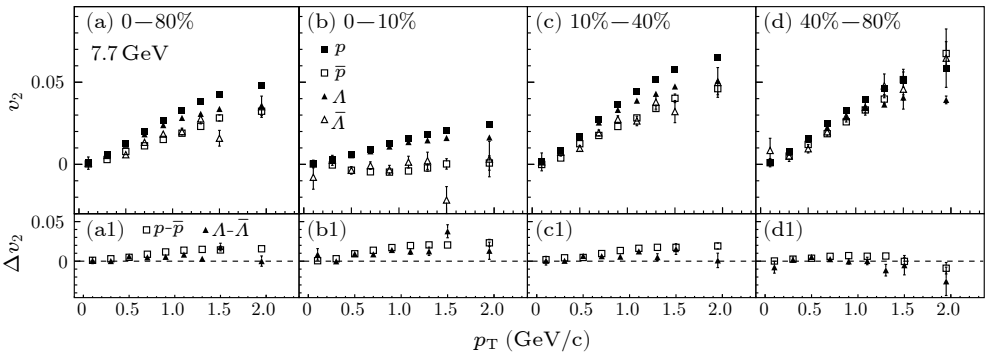

Fig. 1. Plot of v_2 as a function of transverse momentum (p_{T}) for protons, anti-protons, Λ, and $\bar{\Lambda}$ in Au+Au collisions at $\sqrt{s_{\mathrm{NN}}} = 7.7$ GeV for four centrality bins: (a) 0–80%, (b) 0–10%, (c) 10%–40%, and (d) 40%–80%, with a fixed evolution time of 10 fm/c. The bottom panels display the v_2 differences between baryons and anti-baryons as a function of p_{T}.

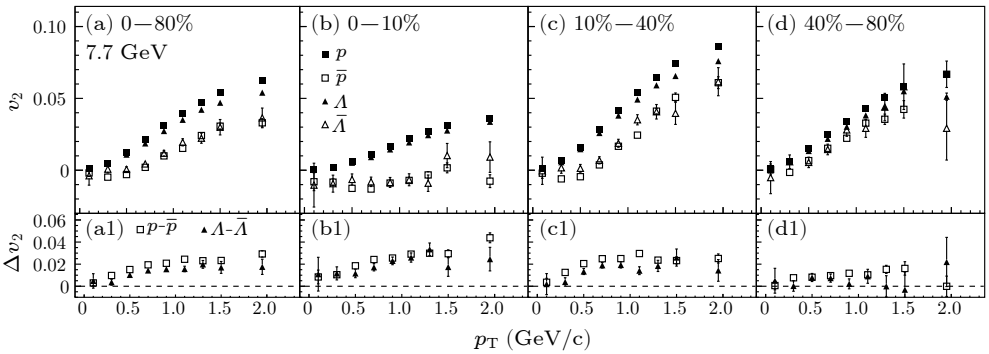

Fig. 2. Plot of v_2 as a function of p_{T} for protons, anti-protons, Λ, and $\bar{\Lambda}$ in Au+Au collisions at $\sqrt{s_{\mathrm{NN}}} = 7.7$ GeV for four centrality bins: (a) 0–80%, (b) 0–10%, (c) 10%–40%, and (d) 40%–80%, with a fixed evolution time of 50 fm/c. The bottom panels display the v_2 differences between baryons and anti-baryons as a function of p_{T}.

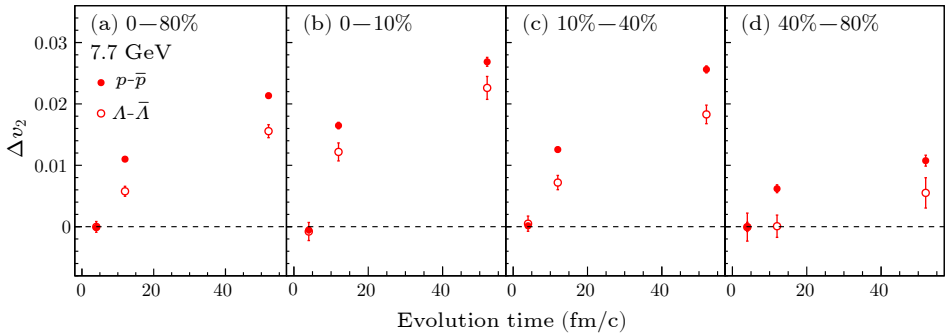

Fig. 3. Plot of v_2 differences between baryons and anti-baryons as a function of evolution time in Au+Au collision at $\sqrt{s_{\mathrm{NN}}} = 7.7$ GeV for four centrality bins: (a) 0–80%, (b) 0–10%, (c) 10%–40%, and (d) 40%–80%.

At an evolution time of 50 fm/c, compared to 10 fm/c, the freeze-out of the particles is mostly complete, and the interactions are sufficient. As shown in panels (a), (b), (c), and (d) of Fig. 2, the v_2 magnitude is larger than that at an evolution time of 10 fm/c. The same conclusion applies to the v_2 differences in panels (a1), (b1), (c1), and (d1) in Fig. 2. Consequently, choosing 50 fm/c provides a clearer and more definitive illustration of the influence of different quark compositions on the proton v_2 and Λ v_2 differences. Over different centrality intervals, the proton v_2 differences are markedly greater than the Λ v_2 differences. This observation further strengthens the evidence for the critical role of the varying quark configurations in the v_2 differences observed in heavy-ion collisions.

Figure 3 shows the extracted results of the proton v_2 and Λ v_2 difference as functions of the evolution time. It is evident that at 2 fm/c, the proton v_2 differences closely resemble the Λ v_2 differences, with both converging near zero

for each centrality bin. As time progresses, the magnitude of v_2 increases and the distinction between the proton v_2 and Λ v_2 differences becomes increasingly significant. Notably, at 10 fm/c and 50 fm/c, the proton v_2 differences exceed the Λ v_2 differences, highlighting a growing disparity between both quantities. As previously discussed, an evolution time of 2 fm/c corresponds to the early stages of a collision. During this early stage, interactions among the particles are rare, and only a few particles are produced. As previously stated, v_2 depends on these interactions. Consequently, at an evolution time of 2 fm/c, the v_2 differences are nearly zero for the four centrality bins. By examining the v_2 differences during the early stages of the collision and at early evolution times, we gain a more comprehensive understanding of the interactions between particles and their impact on the values of v_2 for protons and Λ. These calculations also provide insights into the fundamental dynamics governing the early evolution of the system and subsequent development of v_2.

At an evolution time of 10 fm/c, both proton v_2 and Λ v_2 increase significantly. Simultaneously, the values of v_2 for baryons and anti-baryons show clear differences and increase as the evolution time increases. Considering the composition of different constituent quarks in the anti-proton and $\overline{\Lambda}$, with the proton containing three constituent quarks (uud), the anti-proton consisting of $\overline{u}$, $\overline{u}$, $\overline{d}$ constituent quarks, Λ consisting of u, d, s constituent quarks, and $\overline{\Lambda}$ consisting of $\overline{u}$, $\overline{d}$, $\overline{s}$ constituent quarks, we can delve into the dynamics within the constituent quark paradigm. Particles transported from beam rapidity ($y = y_{\rm beam}$) to midrapidity ($y = 0$) undergo a greater number of interactions, whereas particles and anti-particles produced from vacuum at lower energies are likely to experience fewer interactions. In other words, u and d quarks, which are present from the onset of the collision and experience the transport process, undergo more interactions compared to s, $\overline{s}$, $\overline{u}$, and $\overline{d}$ quarks. In this scenario, it can be inferred that the transported particles exhibit a larger value of v_2. Considering that s quarks are also produced, they may undergo fewer collisions, resulting in lower v_2 values. Therefore, we infer that Λ (uds) v_2 is lower than proton (uud) v_2. Similarly, given that $\overline{u}$, $\overline{d}$, and $\overline{s}$ are produced quarks, the v_2 value for $\overline{\Lambda}$ ($\overline{u}\overline{d}\overline{s}$) is comparable to that of the anti-proton ($\overline{u}\overline{u}\overline{d}$). The v_2 value for the anti-proton ($\overline{u}\overline{u}\overline{d}$) is lower than that for the proton (uud), and the v_2 value for $\overline{\Lambda}$ ($\overline{u}\overline{d}\overline{s}$) is less than that for Λ (uds).

Finally, we compared the SMASH calculations with existing STAR BES-I experimental data. Figure 4 shows the proton v_2 and Λ v_2 differences for different centrality bins in Au + Au collisions at $\sqrt{s_{\rm NN}} = 7.7$ GeV. The blue bands represent the v_2 differences in protons and anti-protons from STAR BES-I in the 0–80%, 0–10%, and 10%–40% centrality bins, whereas the red band represents the v_2 differences for Λ and $\overline{\Lambda}$ from STAR BES-I in the 0–80% centrality range.[35–37] The open blue circles and open red triangles correspond to the results from the SMASH model for proton and Λ v_2 differences, respectively. The fitting ranges used to extract the v_2 differences in the SMASH model are consistent with the STAR BES-I experimental data for each centrality bin. For protons in the centrality bins of 0–80%, 0–10%, and 10%–40%, the $p_{\rm T}$ fitting ranges used are 0.46–1.64 GeV/c, 0.78–1.49 GeV/c, and 0.46–1.64 GeV/c, respectively, consistent with STAR BES-I. For Λ in the 0–80% and 10%–40% centrality bins, we used the same $p_{\rm T}$ fitting ranges as those in STAR BES-I, namely 0.87–1.53 GeV/c and 0.46–1.64 GeV/c. In the 0–10% centrality bin, given that no experimental data are available for Λ Δv_2, we applied the same fitting range as that used for protons to ensure a fair comparison. For the 40%–80% centrality bin, with no STAR BES-I results as a reference, we used the fitting range of 0.60–2.3 GeV/c, following the approach shown in Fig. 3. The default evolution time in the SMASH model is 200 fm/c. Figure 4 shows that the SMASH model quantitatively describes the STAR BES-I experimental data in the 0–10% centrality bins within large data uncertainties. Because of the large statistical errors in the BES-I data, it is not possible to determine whether the model results quantitatively reproduce the data in the 0–80% and 10%–40% centrality bins. Higher statistics from BES-II are needed to address this issue. Given the relatively low statistics and large uncertainties in the STAR BES-I data, it is not possible to definitively determine whether Δv_2 differs between protons and Λ particles. Furthermore, previous research suggests that the effects induced by a strong electromagnetic field may influence the observed v_2 differences.[56,57]

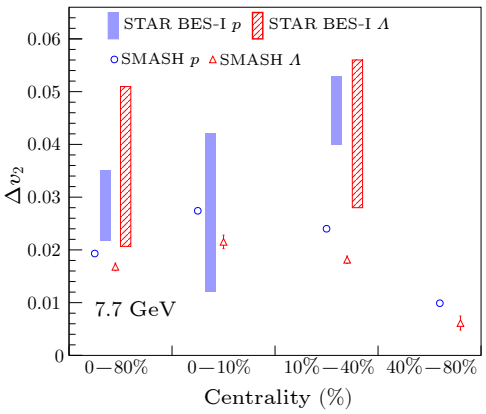

Fig. 4. The v_2 differences between baryons and anti-baryons in Au+Au collisions at $\sqrt{s_{\rm NN}} = 7.7$ GeV are presented for four centrality bins: 0–80%, 0–10%, 10%–40%, and 40%–80%, using the full default evolution time (200 fm/c) in the SMASH model. The model results are compared with experimental data from STAR BES-I.

Most importantly, the proton v_2 differences are greater than the Λ v_2 differences in the SMASH model. The baryon-type dependence of the v_2 differences between baryons and anti-baryons can be explained by the transported and produced particles discussed above. The BES-I data cannot verify or falsify this because the uncertainties are large. New measurements from STAR BES-II will provide experimental data with higher precision and further constrain the models.[40–47]

4. Summary. In this study, we used the SMASH model to analyze the values of v_2 for protons and Λ in Au + Au collisions at $\sqrt{s_{\rm NN}} = 7.7$ GeV as a function of the evolution time. The results indicate that the v_2 differences are nearly zero at 2 fm/c for protons (Λ) and their cor-

responding anti-particles. However, as the evolution time progresses, the disparity between the proton v_2 and Λ v_2 differences becomes increasingly prominent, with the proton v_2 differences surpassing those of Λ. The explanation for this is that protons contain more transported quarks than Λ from a statistical perspective. These transported quarks, which undergo more interactions, exhibit higher v_2 values. As the evolution time increases, more significant differences develop between the Δv_2 values of protons and those of Λ. We compared the Δv_2 values for protons and Λ with the data from the STAR BES-I experiment and observed that the SMASH results quantitatively match the experimental data in the 0–80% and 0–10% centrality bins.

Owing to the statistical limitations of the experimental data, it is not possible to determine whether there are differences between proton and Λ Δv_2 values. The STAR BES-II experiment recorded 12–25 times more events than BES-I for Au + Au collisions at $\sqrt{s_{\rm NN}} = 7.7$–$19.6\,{\rm GeV}$. The forthcoming measurements from STAR BES-II will establish constraints on the model interpretations for the v_2 differences between particles and anti-particles.

Acknowledgements. This work was supported in part by the National Key Research and Development Program of China (Grant Nos. 2022YFA1604900 and 2024YFA1610700) and the National Natural Science Foundation of China (Grant No. 12175084). The numerical calculations were performed on a GPU cluster located at the Nuclear Science Computing Center, Central China Normal University (NSC3).

References

[1] Voloshin S and Zhang Y 1996 *Z. Phys. C* **70** 665
[2] Poskanzer A M and Voloshin S A 1998 *Phys. Rev. C* **58** 1671
[3] Voloshin S A, Poskanzer A M, and Snellings R 2010 *Landolt-Bornstein* **23** 293
[4] Bzdak A, Esumi S, Koch V, Liao J F, Stephanov M, and Xu N 2020 *Phys. Rept.* **853** 1
[5] Luo X F, Shi S S, Xu N, and Zhang Y F 2020 *Particles* **3** 278
[6] Chen J H, Dong X, He X H *et al.* 2024 *Nucl. Sci. Tech.* **12** 214
[7] Abdallah M S, Aboona B E, Adam J *et al.* (STAR Collaboration) 2022 *Phys. Lett. B* **827** 136941
[8] Abdallah M S, Aboona B E, Adam J *et al.* (STAR Collaboration) 2022 *Phys. Lett. B* **827** 137003
[9] Adamczyk L, Adkins J K, Agakishiev G *et al.* (STAR Collaboration) 2017 *Phys. Rev. Lett.* **118** 212301
[10] Adamczyk L, Adkins J K, Agakishiev G *et al.* (STAR Collaboration) 2016 *Phys. Rev. Lett.* **116** 062301
[11] Adamczyk L, Adkins J K, Agakishiev G *et al.* (STAR Collaboration) 2015 *Phys. Rev. Lett.* **115** 222301
[12] Abelev B I, Aggarwal M M, Ahammed Z *et al.* (STAR Collaboration) 2010 *Phys. Rev. C* **81** 044902
[13] Ollitrault J Y 1992 *Phys. Rev. D* **46** 229
[14] Gustafsson H A, Gutbrod H H, Kolb B *et al.* 1984 *Phys. Rev. Lett.* **52** 1590
[15] Aamodt K, Abelev B, Abrahantes Quintana A *et al.* (ALICE Collaboration) 2010 *Phys. Rev. Lett.* **105** 252302
[16] Adler S S, Afanasiev S, Aidala C *et al.* (PHENIX Collaboration) 2003 *Phys. Rev. Lett.* **91** 182301
[17] Chatrchyan S, Khachatryan V, Sirunyan A M *et al.* (CMS Collaboration) 2013 *Phys. Rev. C* **87** 014902
[18] Liu Z W and Shi S S 2024 *Phys. Rev. C* **110** 034903
[19] Zhao S J, Xu H J, Zhou Y, Liu Y X, and Song H C 2024 *Phys. Rev. Lett.* **133** 192301
[20] Jia J Y, Giacalone G, and Zhang C J 2023 *Chin. Phys. Lett.* **40** 042501
[21] Xu Z Y, Liu J L, Zhang P P, Zhang J B, and Lei H 2017 *Chin. Phys. Lett.* **34** 062501
[22] Yan T Z 2013 *Chin. Phys. Lett.* **30** 092501
[23] Yang H Y, Zhou D C, Yang C B, and Cai X 2002 *Chin. Phys. Lett.* **19** 1082
[24] Liu J L, Shan L Q, Feng Q C, Wu F J, Zhang J B, Tang G X, and Huo L 2009 *Chin. Phys. Lett.* **26** 072501
[25] Li N and Shi S S 2011 *Chin. Phys. Lett.* **28** 122502
[26] Wu S J, Shen C, and Song H C 2021 *Chin. Phys. Lett.* **38** 081201
[27] Li P C, Wang Y J, Li Q F, and Zhang H F 2022 *Phys. Lett. B* **828** 137019
[28] Colonna M 2020 *Prog. Part. Nucl. Phys.* **113** 103775
[29] Huovinen P, Kolb P F, Heinz U, Ruuskanen P V, and Voloshin S A 2001 *Phys. Lett. B* **503** 58
[30] Shen C and Heinz U 2012 *Phys. Rev. C* **85** 054902
[31] Zhao W, Ko C M, Liu Y X, Qin G Y, and Song H 2020 *Phys. Rev. Lett.* **125** 072301
[32] Gross D J, Pisarski R D, and Yaffe L G 1981 *Rev. Mod. Phys.* **53** 43
[33] Lin Z W, Ko C M, Li B A, Zhang B, and Pal S 2005 *Phys. Rev. C* **72** 064901
[34] Huovinen P and Petreczky P 2010 *Nucl. Phys. A* **837** 26
[35] Adamczyk L, Adkins J K, Agakishiev G *et al.* (STAR Collaboration) 2016 *Phys. Rev. C* **93** 014907
[36] Adamczyk L, Adkins J K, Agakishiev G *et al.* (STAR Collaboration) 2013 *Phys. Rev. Lett.* **110** 142301
[37] Adamczyk L, Adkins J K, Agakishiev G *et al.* (STAR Collaboration) 2013 *Phys. Rev. C* **88** 014902
[38] Adamczyk L, Agakishiev G, Aggarwal M M *et al.* (STAR Collaboration) 2012 *Phys. Rev. C* **86** 054908
[39] Adams J, Aggarwal M M, Ahammed Z *et al.* (STAR Collaboration) 2005 *Phys. Rev. Lett.* **95** 122301
[40] Tu B, Shi S S, and Liu F 2019 *Chin. Phys. C* **43** 054106
[41] Steinheimer J, Koch V, and Bleicher M 2012 *Phys. Rev. C* **86** 044903
[42] Dunlop J C, Lisa M A, and Sorensen P 2011 *Phys. Rev. C* **84** 044914
[43] Xu J, Song T, Ko C M, and Li F 2014 *Phys. Rev. Lett.* **112** 012301
[44] Hatta Y, Monnai A, and Xiao B W 2015 *Phys. Rev. D* **92** 114010
[45] Liu H, Wang F T, Sun K J, Xu J, and Ko C M 2019 *Phys. Lett. B* **798** 135002
[46] Li P C, Wang Y J, Steinheimer J, Li Q F, and Zhang H F 2020 *Mod. Phys. Lett. A* **35** 2050289
[47] Burnier Y, Kharzeev D E, Liao J F, and Yee H U 2011 *Phys. Rev. Lett.* **107** 052303
[48] SMASH Collaboration, The SMASH website: https://smash-transport.github.io/
[49] Weil J, Steinberg V, Staudenmaier J *et al.* (SMASH Collaboration) 2016 *Phys. Rev. C* **94** 054905
[50] Bailung Y, Rode S P, Shah N, and Roy A 2024 arXiv:2407.17962[nucl-th]
[51] Götz N, Constantin L, and Elfner H 2023 *Workshop for Young Scientists on the Physics of Ultra-relativistic Nucleus-Nucleus Collisions*
[52] Schäfer A, Karpenko I, Wu X Y, Hammelmann J, and Elfner H 2022 *Eur. Phys. J. A* **58** 230
[53] Tarasovičová L A, Mohs J, Andronic A, Elfner H, and Kampert K H 2024 *Eur. Phys. J. A* **60** 232
[54] Petersen H, Oliinychenko D, Mayer M, Staudenmaier J, and Ryu S 2019 *Nucl. Phys. A* **982** 399
[55] Le Fèvre A, Leifels Y, Hartnack C, and Aichelin J 2018 *Phys. Rev. C* **98** 034901
[56] Acharya S, Adamová D, Adler A *et al.* (ALICE Collaboration) 2020 *Phys. Rev. Lett.* **125** 022301
[57] Abdulhamid M I, Aboona B E, Adam J *et al.* (STAR Collaboration) 2024 *Phys. Rev. X* **14** 011028